Proceedings of ASME Turbo Expo 2011
GT2011
June 6-10, 2011, Vancouver, British Columbia, Canada

GT2011-46310

INCLUSION OF AN ESTIMATION METHOD FOR HEAT LOSSES IN THE DESIGN PHASE OF HIGH-PRESSURE TURBINES

Christoph Starke and Heinz-Peter Schiffer
Department of Aerospace Propulsion
Technische Universität Darmstadt
Darmstadt, Germany

ABSTRACT

The paper provides a methodology for the estimation of heat losses in high-pressure turbine stages. Sophisticated aero-thermal analyses require detailed input data in terms of geometry and boundary conditions. Thinking of a turbine design as a continuing process, this data will not be available at an early design stage. On the other hand, in that very stage many decisions are to be taken which have a severe influence on heat losses.

The presented estimation method is based on a simple network of heat resistances. For a design process of a future turbine, the heat resistances have to be calibrated using aero-thermal models or measurements of an existing reference turbine. In a first step, the calibrated resistances will be adapted to the new design using scaling laws based on global parameters such as free-stream velocity and temperature or casing thickness. In the course of turbine design, detailed input data will be available allowing for more complex aero-thermal computations. The results can be used to further improve the heat resistances in order to achieve higher accuracy of the heat loss model.

The scaling laws for the heat resistances are compared to CFD computations of exemplary cases. In the following, the method is applied to a typical design scenario. Both, a reference case and a future design of a high-pressure stator 1 geometry including casing and two secondary flow cavities are set-up as conjugate heat transfer models. The elaborated model is used to estimate the heat fluxes of the future design based on the reference case. A comparison to the conjugate heat transfer results illustrates the accuracy of the method.

NOMENCLATURE

A	Surface area
L	Reference length
$\dot{Q}_e$	Heat flux (internal)
$\dot{Q}_i$	Heat flux (external)
R	Heat resistance
T_c	Coolant temperature
$T_{w,ad}$	Adiabatic wall temperature
T_∞	Free-stream or bulk temperature
d	Solid wall thickness
α	Heat transfer coefficient
η_c	Film cooling effectiveness
λ	Thermal conductivity
Nu	Nusselt number
Pr	Prandtl number
Re	Reynolds number
Tu	Turbulence intensity
$'$	Superscript of reference case quantities

INTRODUCTION

The quest for further improvement of gas turbine engines in terms of less specific fuel consumption and achieving a better thrust-to-weight ratio leads to ambitious challenges in engine design. Until today, the continuous increase of the turbine inlet temperature is a main issue in engine development. Additionally, the ongoing augmentation of the bypass ratio decreases the available space for the high-pressure turbine components. This leads to higher surface-to-volume ratios inside the turbine and consequently tends to higher heat losses.

The general aerodynamic efficiency of modern turbine blading has reached a very high level and the margins for further improvement have decreased significantly. Potential for improvement is expected in the field of interaction between different engine components. In other words, the coupling of different domains in the engine design will have to be enhanced. This will stay an important objective for the aero-thermal design of turbines.

Speaking about the surface temperature of blades and endwalls, the thermal design of turbines is already intensively connected to the aerodynamic design. Especially cooling plays an important role here. But as the heat losses of high-pressure turbines already reach a respectable amount of the power output and still tend to increase, this will be another aspect worth considering in the aerodynamic design. The consideration of heat losses can be split into two parts: quantification and consequences.

Publications dealing with the consequences of heat losses in turbines or with the thermodynamic cycle of the whole engine in general are rare. The common way to describe non-adiabatic cycles is based on the assumption that the irreversibilities of the adiabatic case remain constant for the non-adiabatic case. This simplification allows to overlay the entropy change due to heat fluxes. Atkins and Ainsworth [1] used such an approach for a straight-forward estimation of the adiabatic turbine efficiency based on measurements under non-adiabatic conditions of a 1.5-stage test rig. They showed that the heat loss influence on irreversibilities of the process is negligible, even for heat losses up to 4% shaft power. In engine design, the consequences of turbine heat losses must also be seen in the context of the thermodynamic engine cycle. Therefore, Young and Wilcock [2, 3], El-Masri [4] and Gulen [5] presented several thermodynamic formulations of multi-stage turbines affected by heat losses and cooling. However, these models simply introduce the external heat losses per blade row as a scalar value. It is proposed to determine the value by using an adequate Nusselt number correlation.

For the quantification of heat losses, this correlation-based estimation might be sufficient in the early pre-design phase. But a more sophisticated model would be necessary thereafter. During the aerodynamic design, a heat loss model should enable the engineer to evaluate the influence of his design decisions on the turbine heat losses. Literature provides a vast number of different Nusselt number correlations for nearly all flow structures in a turbine. The applications range from general cases like duct flows up to special geometries like knife seals, for example. But the experience shows that even with highly specialised Nusselt number correlations the accuracy is not sufficient to judge different design alternatives. The use of computational fluid dynamics (CFD) has become very common for heat transfer analyses over the last two decades. However, the analyses are often limited to the calculation of the fluid-side heat transfer coefficients. Of course, a decrease of heat transfer coefficients will most likely cause a decrease of heat losses. But an analysis limited to the fluid-side will be unable to quantify the heat losses in an energetic way.

Coupled aero-thermal methods like the conjugate heat transfer method (CHT) extend standard CFD by additionally solving the energy equation in solid regions and coupling fluid and solid parts on their interfaces. First, CHT computations were often performed for isolated geometry features, such as arrangements of film cooling holes or blade tips. But recent publications show a clear trend towards more geometrical and physical complexity, such as a whole stage model from Sipatov et al. [6] or the consideration of unsteadiness by He and Oldfield [7]. Regardless, a pure CHT model is not suitable for the structural complexity of a whole turbine. Okita [8, 9] presented a rotor CHT model where parts of the secondary flow have been modelled by correlations as they turned out to be corruptive for the convergence. In contrast, state-of-the-art industrial thermal models mostly obtain the fluid-side Nusselt numbers by one-dimensional flow models. In terms of accuracy, they normally exceed CHT models as they have been calibrated for years with former test results.

In summary, it can be stated that there are well established methods available which allow for reliable coupled aero-thermal analyses.

OBJECTIVES OF THE ESTIMATION METHOD

The remaining problem is the time-dependent availability of the input data during the design phase. The flow structure in the hot-gas path results from the aerodynamic design. In a typical turbine design process, it can be obtained in a very early stage. The solid heat resistances cannot be obtained unless the solid components are designed. This task normally follows the aerodynamic design. Therefore, the engineer may not use this information during the aerodynamic design process. This applies also to the design of the secondary air system. However, many decisions having a severe effect on heat losses have to be taken in that early aerodynamic design. But coupled aero-thermal computations are performed at an rather advanced stage of the turbine design progress. The computations can account for heat losses, whereas the possibilities to counteract are limited.

The question is, how far the available methods can be used at the start of a turbine design process. This work presents an approach to an estimation method aimed at enabling the aerodynamic design engineer to comprehend the influence of his decisions on heat transfer. The quantification of heat losses is done by means of a modular network of heat resistances. It is split into two independent sub-steps, each resulting in an estimation of the energetic heat losses. First, the unknown parameters are obtained by scaling existing results from similar preceding turbine designs.

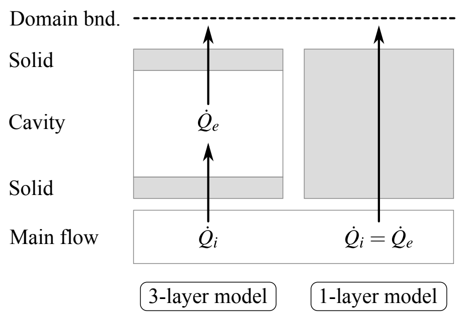

FIGURE 1. Heat flux layer models

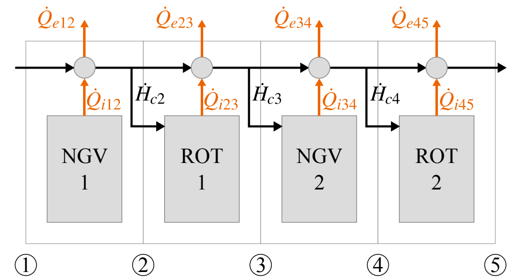

FIGURE 2. Global heat loss model

During the development of the new design, more detailed input data (e. g. CFD results) will be available and, in a second step, the parameters estimated in the first step can now be amended leading to an improved second prediction. The analysis of the thermodynamic consequences for the turbine and for the engine cycle is well established in the papers cited above and will therefore not be addressed here.

MODEL FORMULATION

The turbine domain which is subject of the presented heat loss model consists of the hot-gas path, its end-walls, the surrounding cavities of the secondary air system and the outer casing of the cavities. The heat which passes through the outer casing is most likely picked up by the bypass flow. As the bypass mass-flow has a higher order of magnitude, its temperature increase is neglected and the heat is assumed to be lost. The heat fluxes out of the domain are referred to as external heat losses. The heat losses from the hot-gas path into the end-walls are referred to as internal heat losses.

As a first simplification, one-dimensional heat flux is assumed. Consequently, there are two possibilities: Either the internal heat flux is picked up by the secondary air system and only a part of it is lost as external loss on the other side of the secondary air system cavity ($\dot{Q}_i > \dot{Q}_e$), or the whole internal loss directly exits the defined turbine domain as external loss ($\dot{Q}_i = \dot{Q}_e$). The annulus can be described by independent axial sections of both cases as shown in Figure 1.

All boundary layers and solid walls are represented by a heat resistance. For boundary layers this is defined as

$$R = \frac{1}{\alpha A} \tag{1}$$

and for solid walls

$$R = \frac{d}{\lambda A} \tag{2}$$

Figure 2 shows a model built up for a two-stage high-pressure turbine with one secondary flow path. For each cavity indicated by the grey circles, the difference between internal and external losses leads to the temperature change of the passing fluid. The temperature change affects the driving temperatures in all subsequent cavities (see black arrows). One part of the flow is passing to the secondary air cavities of next blade row and the other part is used as coolant and is injected into the main-flow. As both parts do not necessarily have the same temperature in reality, a so-called power-split factor has to be introduced determining the repartition of the heat input.

The quantification finally results in equations expressing the accumulated internal and external heat losses per blade row. The remaining task is the estimation of all heat resistances and the driving fluid-side temperatures.

HEAT RESISTANCE ESTIMATION PROCEDURE

A very common practice for engineering computations is to start from a well-known reference case. Whereas the computation of one case includes many sources of errors, the general experience shows that the difference to a computed reference case normally shows good agreement compared to the difference in reality. New turbine designs are normally based on existing turbines. It can be supposed that enhanced aero-thermal models, probably even measurements of preceding comparable turbines are available at the beginning of a new turbine design process. Thus, the presented prediction method is always based on data of a comparable existing turbine which will be referred to as "reference turbine" in the following. The new turbine to be analysed will be referred to as "future turbine".

With the abstracted model described in the preceding chapter it is not possible to directly calculate the heat losses of a turbine stage. The simplifications are too strong to represent reality. The most important assumption of the present heat flux model is that for two comparable turbines the change of heat losses will mainly depend on the driving temperatures and the few factors of Equations (1) and (2). Hence, if a model is available which can calculate the known heat losses of an existing turbine, the heat losses of the new turbine can be estimated by adapting these

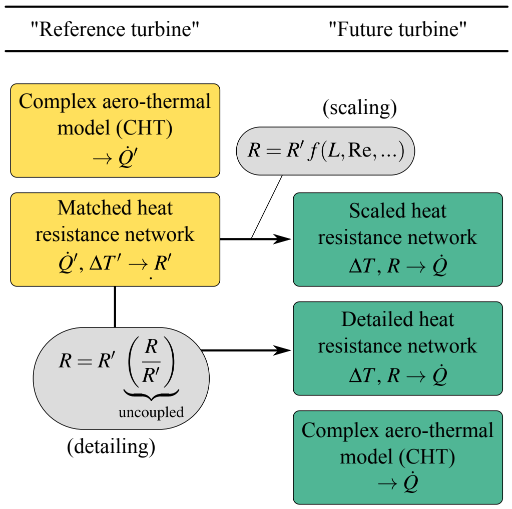

FIGURE 3. Estimation procedure

factors.

Figure 3 illustrates the estimation procedure. The heat loss model has to be set up for the reference turbine first. This step will be called "matching" and results in a heat resistance network which is used to calculate the heat losses $\dot{Q}'$ of the reference turbine. In the first iteration cycle, the heat resistances and driving temperatures of the future turbine are obtained by scaling all the corresponding values of the reference case. This is the most complex task, called "scaling", and it will be typically done in the early design phase. Despite the lack of detailed input data, the scaling gives a first estimation of the expected heat losses. With proceeding design, it must be possible to incorporate the results of detailed studies such as CFD computations into the estimation model. This step will be called "detailing". The detailed model gives a second, improved estimation of the future turbine heat losses. The three steps are briefly described in the following.

Step 1: Set-up and Matching

The matched heat loss model must be able to calculate the heat losses of the reference turbine. The following information has to be provided from the thermal model of the reference case:

1. Temperatures at the domain boundaries
2. Fluid-side temperatures of the hot-gas path and the cavities
3. All heat fluxes $\dot{Q}_i$ and $\dot{Q}_e$

The fluid-side temperatures are representing the so-called recovery temperatures or adiabatic wall temperatures. For high-speed flows, the adiabatic wall temperature is obtained by correcting the free-stream temperature with a factor to account for the the non-isentropic compression next to the wall [10]. Especially for the first stator, the incident hot-gas flow distribution is not uniform due to combustor hot-spots. Wilcock et al. [11] therefore used a correction factor proposed by Kawaike et al. [12].

Additionally, turbine blades and end-walls are normally film-cooled. The coolant protects the component surfaces against the hot-gas mainly by decreasing die adiabatic wall temperature. Following the work of Young and Wilcock [3], the adiabatic wall temperature is expressed as function of the free-stream temperature, the coolant temperature and the film cooling effectiveness:

$$T_{w,ad} = T_\infty + \eta_c \left(T_c - T_\infty\right) \tag{3}$$

Provided that the temperatures and heat fluxes of the reference turbine are known, the resistances and accordingly the heat transfer coefficients and conductivities can be determined directly.

Step 2: Scaling

The most difficult task is the adaptation of the matched heat loss model to the new turbine design. All fluid-side temperatures and heat resistances in the model have to be adapted using the available global parameters.

The fluid-side heat resistances depend on the area of the wetted surface and the heat transfer coefficient. While the adaptation of the area is just a geometrical issue, the appropriate scaling of the heat transfer coefficient is a more critical point. Heat transfer coefficients can be estimated using Nusselt number correlations. Here, it is not necessary to find an explicit correlation for each of them. As the resistances of the matched model are known, it is sufficient to find suitable scaling laws. The most general form of a Nusselt number correlation is:

$$\mathrm{Nu} = C\,\mathrm{Re}^n\,\mathrm{Pr}^m = \frac{\alpha L}{\lambda} \tag{4}$$

Supposing that the Prandtl number remains unchanged, the heat transfer coefficient of all surfaces of the new turbine can be estimated by scaling the heat transfer coefficient of the reference turbine surfaces with the Reynolds number ratio powered by an exponent n. The geometrical influence leads to further scaling factors and the scaled heat resistance can be written as:

$$R = R' \frac{A'}{A} \frac{L}{L'} \left(\frac{\mathrm{Re}'}{\mathrm{Re}}\right)^n \tag{5}$$

The quantities of the reference case are labelled with primes. For clarity, constant gas properties are supposed. A comparable scaling approach was also used by Kawaike et al. [12] for the estimation of mid-span blade heat transfer coefficients.

Following the global formulation of the Nusselt number correlation for a flat plate flow, the Reynolds number is based on the surface length in direction of the flow. In case of a turbulent

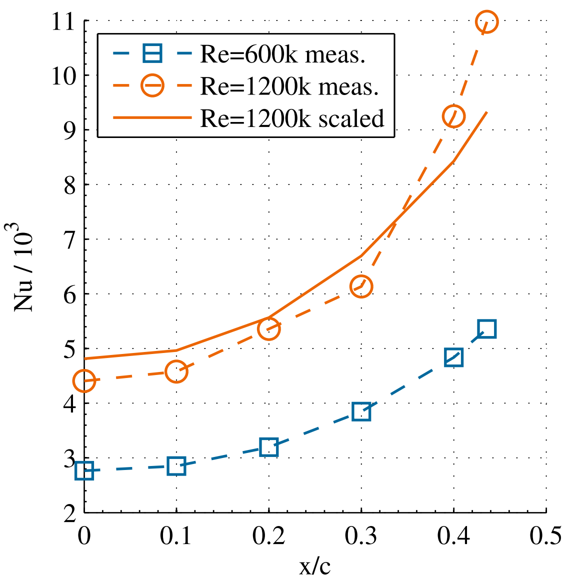

FIGURE 4. Pitchwise-avg. Nusselt numbers (Kang et al. [13])

boundary layer, the exponent n is equal to 0.8. According to Lakshminarayana [10], most of the Nusselt number correlations found in the literature have an exponent n ranging from 0.6 to 1.0. But Lakshminarayana also stated that there is no suitable correlation for blade and end-wall Nusselt numbers yet.

Kang et al. [13] measured end-wall heat transfer in a stator cascade for two different Reynolds numbers. The dashed lines in Figure 4 show pitchwise-averaged Nusselt numbers for $\mathrm{Re} = 600\mathrm{k}$ and $\mathrm{Re} = 1200\mathrm{k}$ which are derived from published data. The solid line is obtained by scaling the low-Reynolds result by $2^{0.8}$. The scaling slightly under-predicts the change in the front part of the passage by 8% while in the rear part, an over-prdiction of 17% is found. Given that the doubled Reynolds number is a severe change, using $n = 0.8$ for end-wall Nusselt numbers seems to be a good first guess. However, this scaling approach is a strong simplification. It will be verified in the following chapter.

The heat resistances of the solid components can be estimated by introducing scaling factors for each parameter of the solid resistance in Equation (2) leading to the following expression:

$$R = R' \frac{d}{d'} \frac{A'}{A} \frac{\lambda'}{\lambda} \tag{6}$$

If the thickness varies along the axial coordinate, which is normally the case for realistic components, the average thickness has to be used to determine the correct value for d. This is valid as one-dimensional heat transfer is assumed.

Modified film-cooling of the future turbine will have two effects. The major effect is the altered protection of the component surfaces against the hot-gas. This effect is described by Equation (3) and can be included in the estimation as soon as information about the film cooling effectiveness of the future turbine is available. The second effect is that the film-cooling disturbs the passage flow. Hence, a different film-cooling configuration is likely to affect the heat transfer coefficient on the respective surfaces. The changing disturbance between the reference case and the future turbine is not included in the estimation but is believed to play a minor role.

Step 3: Detailing

In the course of progressing design, detailed results like three-dimensional CFD of the hot-gas path or thermal FEM models of solid components will be available. These results can be used to enhance the prediction quality of the heat loss model.

First, three-dimensional CFD from the hot-gas path will be available. Using wall temperature boundary conditions, end-wall heat transfer coefficients can be directly derived for the new turbine. The derived CFD heat transfer coefficients are based on simplified uncoupled models where the choice of the thermal boundary conditions significantly influences the result. However, it can be assumed that, performing one uncoupled CFD computation for the reference case (R') and one for the future turbine (R), the ratio between the resulting heat resistances will be reliable even for the coupled case. Hence, it is advised to replace the scaling factor of the respective surfaces in the heat loss model by the ratio of the two computed uncoupled heat resistances. Based on the heat resistance of the reference turbine R', the resistance of the future turbine can be estimated by the following expression:

$$R = R' \underbrace{\left(\frac{R}{R'}\right)}_{\text{uncoupled}} \tag{7}$$

This approach is also valid for solid heat resistances which can be derived from uncoupled thermal models.

Example of Application

An illustrative example of application can be given based on the work of Granovskiy et al. [14] who analysed the efficiency potential of several turbine rotor casing treatments. From the published data, the shaft power increase of the best performing casing treatment is estimated as 0.5%. But it is evident that the casing treatment will increase the heat losses. A rough estimation based on the methodology used by Atkins and Ainsworth [1] yields that a heat loss increase of about 1% shaft power would outweigh the improvement. The penalties in the subsequent stages are not comprised.

In a turbine design process, it is essential to be be aware of this problem. Normally, uncoupled CFD computations are performed to calculate the hot-gas side heat transfer coefficients on the casing. But how can a changing heat transfer coefficient be related to an expected efficiency improvement? The scaling procedure of the present heat loss model provides a basic estimation of all heat resistances in the turbine. By embedding the computed heat transfer coefficients into this heat resistance network (detailing), the energetic heat losses are estimated.

SCALING VALIDATION

Different cases have been studied to asses the prediction quality of this Reynolds-based scaling: The first test case is based on heat transfer measurements of the VKI cascade, presented by Arts and Lambert de Rouvroit [15]. The measurements serve as validation of the CFD set-up of the present work. Furthermore, the passage flow at mid-span determining the measured heat transfer is two-dimensional which poses a basic validation case for the Reynolds-scaling. But from an energetic point of view, the end-wall heat transfer is more interesting. The near-wall flow at hub and shroud is decisively affected by three-dimensional secondary flow phenomena representing a more challenging task for the scaling approach. For this reason, the scaling approach is compared to end-wall heat transfer predictions gained by CFD computations of a stator 1 geometry affected by changes of blade count, span and shape. Finally, the capability of the scaling approach is validated for a representative cavity.

VKI Cascade

The VKI cascade is a two-dimensional blow-down cascade where heat transfer measurements at mid-span are published in order to provide a CFD test case. A CFD model is set up using the commercial solver Fine/Turbo by Numeca International. The used solver is a coupled flux based three-dimensional RANS solver. All solutions are obtained in steady state. The presented results are computed using a Spalart-Allmaras turbulence model with and without transition modelling (global transition model, Abu-Ghannam and Shaw [16]). Each published case is calculated. The cases no. 224, 235 and 239 ($Ma_2 = 0.9$, Tu = 6%) come closest to the flow conditions of the in-service stator used below. The transitional result of the Re = 1.2M case agrees well with the measurements. A comparison of the local heat transfer coefficient is shown in Figure 5.

Heat transfer coefficients are computed for all three cases. Based on the Re = 1.2M case, heat transfer coefficients of the Re = 0.6M and Re = 2.4M cases are additionally estimated using the scaling approach. Figure 6 compares surface-averaged Nusselt numbers on pressure and suction side. The average heat transfer coefficients on the pressure and suction side are indicated by the orange asterisks and crosses for the transitional case and by blue circles and boxes for the fully-turbulent, respectively. The lines show the predicted Nusselt number obtained by Reynolds-scaling. Again, orange designates the transitional case and blue the fully-

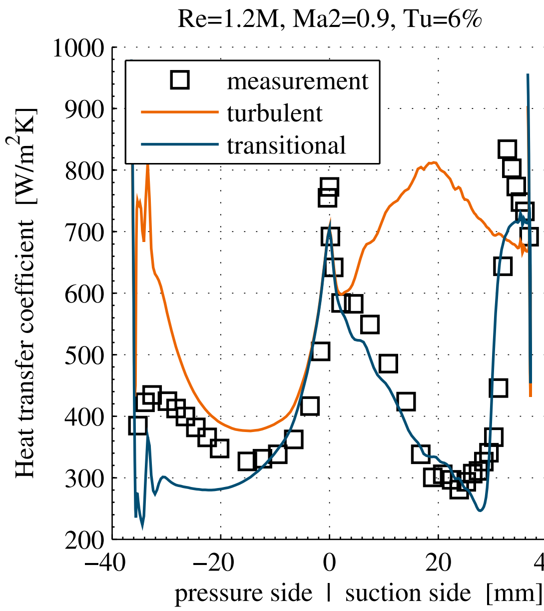

FIGURE 5. Heat transfer coefficient at mid-span (VKI cascade)

turbulent one. For the transitional case, an under-estimation of 23% can be seen on the suction side at Re = 2.1M. On the one hand, the Reynolds-scaling with $n = 0.8$ over-predicts the augmentation of the Nusselt number in the laminar region as $n = 0.5$ would be more adequate here. This would lead to an over-prediction by the model for this point. But the tendency is more than compensated by the fact that in the CFD computation, the transition point where the Nusselt number strongly increases moves upstream decreasing the length of the laminar boundary layer region. Generally, the Reynolds-based scaling cannot cope with complex flow phenomena, e. g. transition. In contrast, the fully-turbulent CFD solution can be very well predicted by Reynolds-scaling. The scaling results (blue lines) agree well with the CFD results (blue circles and boxes).

3D Stator

The second CFD model is set up to evaluate the scalability of the end-wall Nusselt numbers at hub and shroud. Therefore, a first stator of a real in-service flight engine turbine is used as geometry.

End-wall transition stays an unexplored domain in CFD. Even if recent local transition models (see Langtry and Menter [17, 18]) would allow for end-wall transition, no experience regarding the validity is published yet. In this work, all end-walls are assumed to be fully-turbulent. This simplifies the scaling of the Nusselt numbers and is still standard in research and industry.

The variation of the inlet Reynolds number shows the same behaviour as the VKI case and is not shown here. Next, geo-

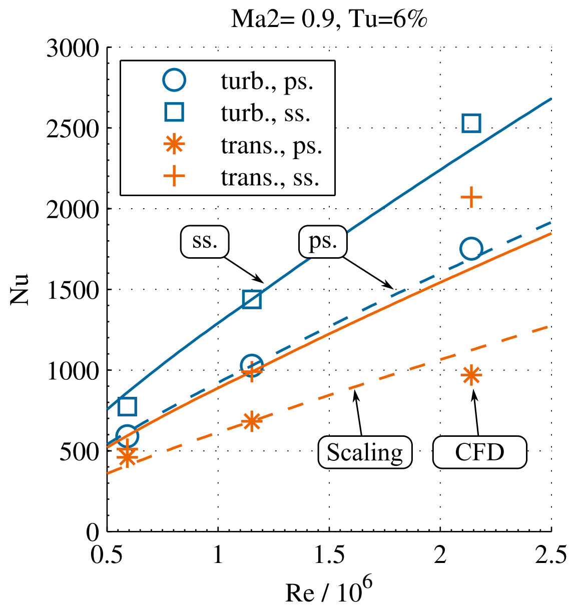

FIGURE 6. Variation of inlet Reynolds number (VKI cascade)

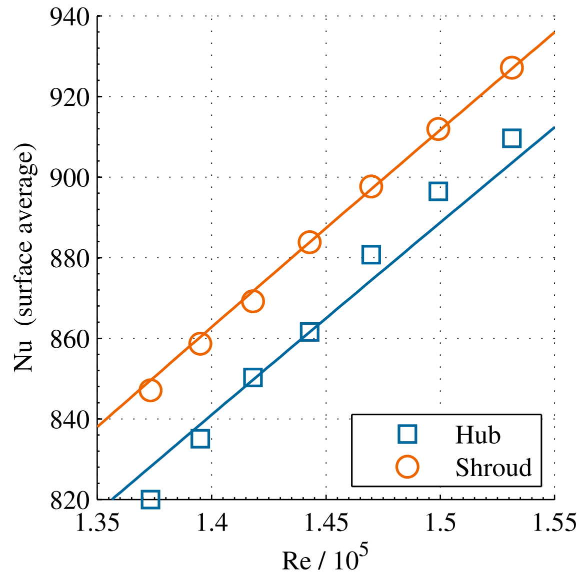

FIGURE 7. Variation of blade number

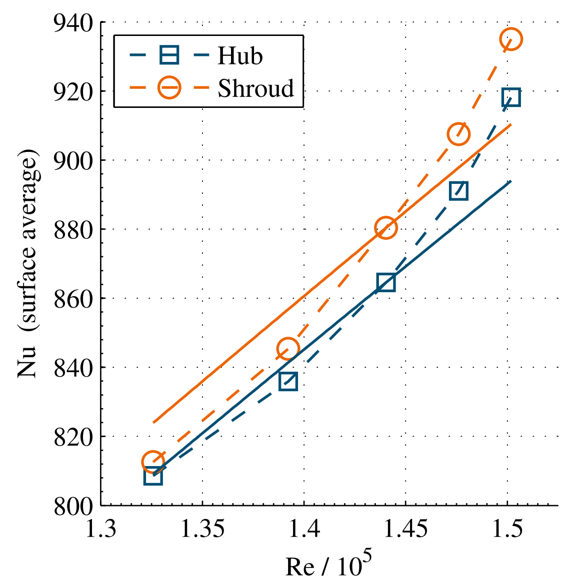

FIGURE 8. Variation of blade span

metrical parameters are changed. The tested range of Reynolds numbers is much smaller than for the variation of inlet boundary conditions. But in the authors' opinion, the range is realistic as the strength of tested geometry variations is oriented on consecutive real engine designs.

Figure 7 shows the average Nusselt number on hub and shroud (squares and circles). Based on the Re = 145k case, the blade count is changed from 37 to 43, each point represents one blade count. As a consequence, the Reynolds number changes due to varying blockage causing different main-stream velocities. Again, the Reynolds-based scaling indicated by the two solid lines predicts the Nusselt number with reasonable accuracy. A further variation provokes heavy separation or blockage. This can neither be handled by the scaling approach, nor is it a design intent.

Then, the channel height is increased and decreased by two discrete steps of 10% for the same stator. By span variation, the pitch-to-span ratio varies from 0.67 to 1.01. The blade geometry is radially scaled to fit in the adapted annulus. Figure 8 shows the CFD results of the hub and shroud Nusselt numbers (squares and circles) compared to the results obtained by Reynolds-scaling of the reference case at $Re \approx 145$k (solid lines). The scaling of the blade has a stronger influence on the flow pattern, especially on the vortex structure, than the change of the blade count. Nonetheless, the Nusselt number can be predicted with reasonable accuracy.

Also the Nusselt number of the second stator of the same turbine is estimated by scaling the model of the first stator in order to assess the prediction quality in case of significant changes in geometry and boundary conditions. The second stator has different flow angles and geometry. The inlet Reynolds number is 164% of the first stator. The CFD computations predict a Nusselt number increase of 53% compared to 48% predicted by the scaling method. An overview of the data is given in Table 1. The estimation error appears reasonable taking into account the severe geometric differences between the two stators.

Quantity	Stator 1	Stator 2
Span	1.00	1.22
Axial chord	1.00	1.28
Re_1	1.00	1.64
Nu (CFD prediction)	1.00	1.53
Nu (estimated by scaling)	1.00	1.48

TABLE 1. Stator 2 heat loss estimation

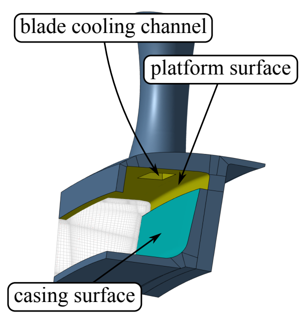

FIGURE 9. Representative hub cavity

Cavities

Finally, the scaling is tested for cavity geometries. Therefore, a representative stator hub cavity as shown in Figure 9 is fed with a varying inlet mass flow. The scaling is based on the inlet Reynolds number of the cavity. Figure 10 compares the average Nusselt number predicted by CFD (squares and circles) with the scaling approach (solid lines). The comparison is made for the platform and casing surfaces of the cavity. The stator platform is located on top of the cavity while the casing represents the inner boundary. The prediction quality is higher at the platform surface of the cavity. In the CFD solution, it is observed that the coolant enters the cavity and passes to the stator plenum which is the outlet of the computed domain. All stream lines are close to the platform surfaces while a big vortex develops between the stream lines and the major part of the casing surface. The velocity level in the vortex hardly depends on the inlet Reynolds number of the coolant supply and so does the casing Nusselt number.

Comparable behaviour was observed in other cavities which have been analysed prior to this work. It turned out that the Reynolds-based scaling is difficult in cavities as often, the flow structure is not dominated by a strong main flow and complicated vortex structures develop. This also poses a challenge to CFD solvers. But in absence of a better approach, the scaling will also be used for cavities in the following.

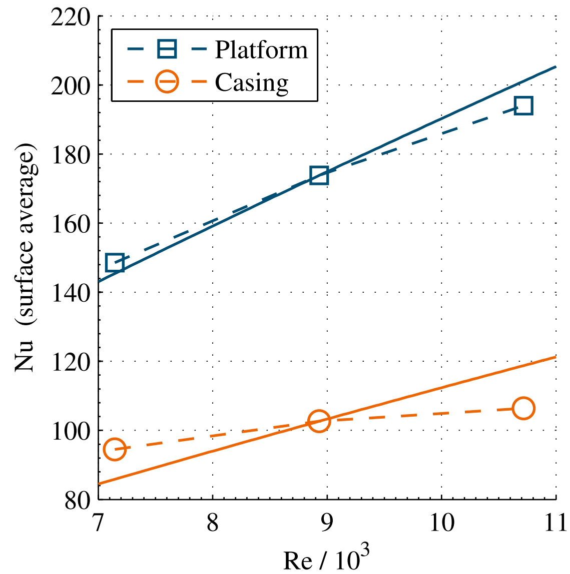

FIGURE 10. Variation of hub cavity mass flow

COUPLED MODEL VALIDATION

This chapter demonstrates the elaborated heat loss model by a simple test scenario of a stator 1 design.

A simplified version of a real in-flight stator 1 geometry including two secondary flow cavities is used as reference case. The future turbine is derived from the reference turbine by an arbitrary variation of geometry and boundary conditions. The geometry, shown in Figure 11, is adapted in order to follow the trend of decreasing core sizes. The mid-span radius is decreased by 5%, the span by 10%, respectively. The pitch decrease is compensated by eliminating 2 blades resulting in a slight pitch increase of 1.5%. The blade thickness and flow angles remain unchanged. The shroud cavity is radially scaled to fit in the new annulus contour posing an easy validation case for the scaling approach. The hub cavity is re-designed leading to a different channel height at the inlet and an adapted shape of the casing flange. This cavity represents a more complicated validation case for the scaling approach. The inlet total pressure is increased by 12%, the inlet total temperature by 5%, respectively. The hub cavity mass-flow is considerably increased by 50%. The adaptations correspond to the order of magnitude validated in the precedent chapter.

In a real design process, a thermal model of the reference case is supposed to be available from the beginning. The heat loss estimations would be based on that model as shown in Figure 3 and would enable to roughly predict the turbine heat losses until a more exact thermal model of the future turbine would come up at an advanced stage of the design process. For the present validation case, two CHT computations are performed serving as thermal models. The CHT model of the reference case is used to

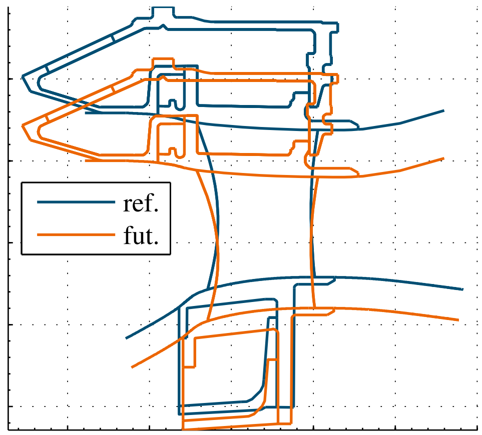

FIGURE 11. Meridional view of the turbine geometry (reference and future design)

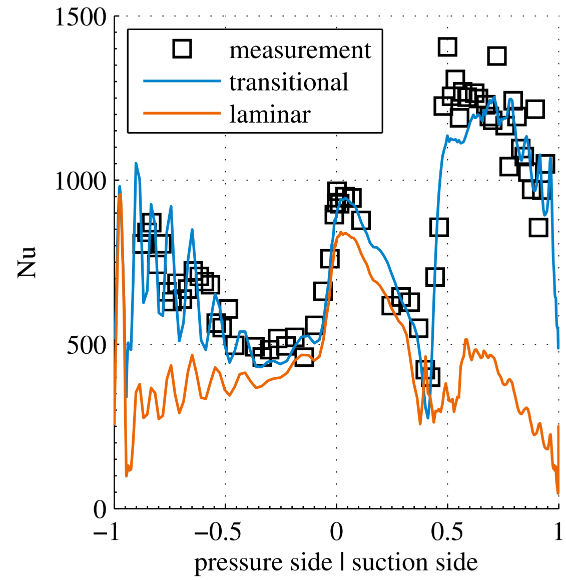

FIGURE 12. Nusselt number distribution at mid-span (MARK-II cascade)

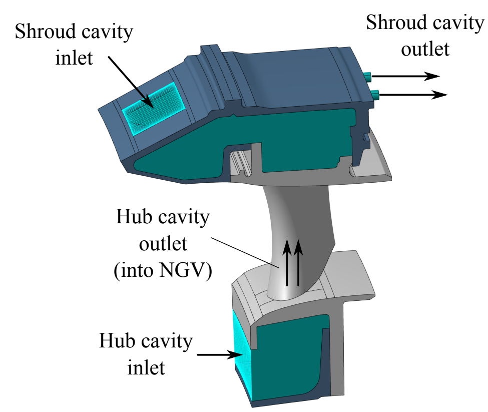

FIGURE 13. CHT stator model

calibrate the heat loss model. The detailing and scaling step lead to two estimations of the stator heat losses. The CHT model of the future turbine is not necessary for the estimation procedure. It is set up to validate the estimations giving a measure of their accuracy.

Numerical Set-up

Also for the CHT computations, the software package Fine/Turbo is used. The turbulent viscosity is again modelled using the one equation Spalart-Allmaras turbulence model. Despite the trend of more complex turbulence models, especially when dealing with heat transfer, the Spalart-Allmaras model is chosen to achieve stable convergence which is found to be more important in the present case.

Prior to the set-up of the stator 1 CHT models, the approach had to be validated. In 1983, Hylton et al. [19] published temperature measurements at mid-span of the MARK-II cascade. The blade Nusselt number distribution was derived from the temperature using a thermal model of the blade solid. A CHT model of this cascade is set-up as validation case. Therefore, the passage including the blade solid is meshed. Mesh size as well as near-wall resolution are kept in the same range as for the stator 1 models. The presented results are based on the 4421 case ($\mathrm{Re}_2 = 2\mathrm{M}$, $\mathrm{M}_2 = 0.9$, $\mathrm{Tu} = 8.3\%$ and $T_w/T_g = 0.7$). Due to the obvious transitional behaviour, an Abu-Ghannam and Shaw transition model must be used like for the VKI case. Figure 12 compares the measured and the predicted Nusselt number distribution ad mid-span which agree reasonably well.

Figure 13 shows the investigated geometry of the stator CHT models. The models contain three fluid domains: the passage of the hot-gas path, the shroud cavity and the hub cavity. The fluid domains are surrounded by four solid domains. The inner and outer end-wall (light grey) separate the two cavities from the hot-gas path. The inner and outer casing (dark grey) are positioned between the cavities and the boundaries of the CHT model.

The computational mesh of the fluid and solid domains is block-structured. The passage consists of 2 million cells. Shroud and hub cavity consists of 1.6 and 0.5 million cells, respectively. In all fluid domains, the near-wall resolution was chosen to achieve a normalised wall distance of $y^+ \approx 1$. Including the four solid domains, the CHT mesh consists of 4.6 million cells. The mesh resolution is equal for both CHT models and is in line with the validated MARK-II case. In contrast to the validation case, the boundary layers of the non-adiabatic walls are modelled as fully-turbulent. This is due to the solver which does not allow for

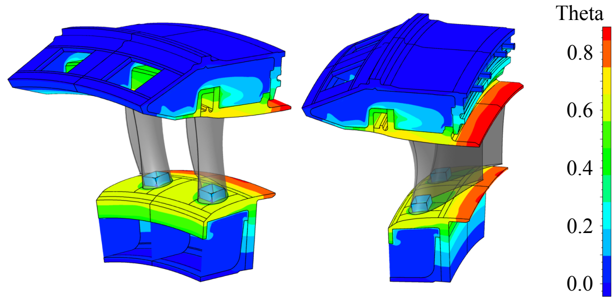

FIGURE 14. Normalised temperatures of the CHT model

transition modelling on end-walls.

As shown in Figure 13, the air injected into the shroud cavity is completely directed towards two discrete holes representing the outlet towards the rotor cavity. Additional cooling flows are not modelled. The air of the hub cavity is ejected into the blade to serve as coolant. Admittedly, the cooling channels inside the blade are not modelled and the blade surface is supposed to be adiabatic. Prior to this work, CHT models have been set-up including the solid blade and the cooling flows, but the huge complexity of the flow led to poor and oscillating convergence which was devastating for the accuracy of the computed heat fluxes. The cold side heat transfer could be modelled by correlations. But the heat losses from the hot-gas path into the blade wall are mainly picked up by the coolant and directly re-injected into the main-flow. From an energetic point of view this means that the heat remains inside the passage. Hence, the blade walls are considered adiabatic.

Results

The CHT computations predict an increase of the main-flow heat losses by 15% compared to the reference case. All heat fluxes are tracked during the computations to ensure convergence. The oscillation amplitudes of all surface heat fluxes are used to assess the quality of the computation results. The maximum oscillation is 0.07% for the internal heat losses and 0.3% for the external ones. Figure 14 gives an impression of the temperature field. The temperature is normalised by the difference of the hot-gas inlet temperature and temperature boundary condition at the outer casing surface.

First, an estimation of the heat losses is conducted following the scaling procedure based on a heat resistance network which is calibrated with the results of the reference case CHT model. The estimated end-wall heat losses on hub and shroud are compared to the results of the future turbine CHT model. The first two bars in both plots of Figure 15 show the prediction error of the scaled heat loss model. The first plot shows the so-called difference error. It is defined as the difference in heat loss between the estimation and

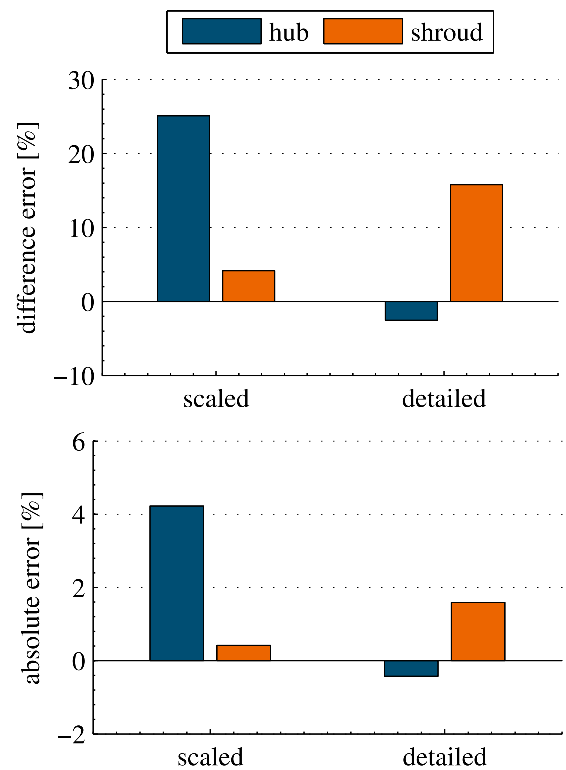

FIGURE 15. Accuracy of estimated end-wall heat losses

the CHT model normalised by the difference in heat loss between the two CHT computations. Compared to the difference predicted by the CHT models, the scaled heat loss model over-predicts the change by 25% at hub and 4% at shroud. The second plot shows the absolute error which is the difference between estimation and CHT model, normalised by the absolute heat losses of the future turbine CHT model. It can be seen that the scaled model over-predicts the hub and shroud heat losses by 4% and 0.4%, respectively.

The discrepancy of the prediction quality between hub and shroud is evident. It can be explained by the fact that, apart from a geometrical scaling factor, the shroud cavities of the two turbines are equal. In contrast, the geometry of the hub cavity is changed in such a way that also the relative size between different geometry features differs. This seems to impair the quality of an estimation by scaling. Indeed, the scaled heat resistances of the hot-gas side and the hub end-wall have an error smaller than 4% compared to the CHT while the heat resistance of the cold-side in the hub cavity is under-predicted by 14%.

Second, an estimation following the detailing procedure is performed. In a real design process, the former scaled resistances would be successively exchanged by resistances obtained by detailing. It is not necessary to replace all of them. But heat resistances which are believed to be critical should be replaced when the required data is available. This should lead to a continuously increasing accuracy during the design process. For the present validation case, two uncoupled CFD computations of the hub cavity solely are performed with isothermal boundary conditions at the domain walls. According to Equation (7), the resistance of the matched heat loss model is scaled by the ratio of the heat resistances of the two uncoupled computations. As a result, the error changes from the under-prediction of 14% to an over-prediction of 8%. Uncoupled CFD computations of the main flow do not lead to an improved estimation of the hot-gas side heat resistances. The error remains constant below 4%. The blue bar on the right-hand side in both plots of Figure 15 shows the prediction errors of the heat losses at the hub. The detailing procedure improved the accuracy leading to a slight under-prediction of the heat loss difference by 2.5%.

In contrast, the detailing procedure of the shroud cavity does not lead to an improved prediction accuracy. Both procedures, the scaling and the detailing, estimate the solid and the cold-side heat resistances with an error of approximately 1%. The heat resistance of the shroud hot-gas side estimated by scaling is 100.4% of the value computed by the future turbine CHT model. But the detailing via two uncoupled main flow CFD computations estimates the resistance to 96.5% of this value. This error is responsible for the unexpected increasing over-prediction of the shroud heat losses (absolute error 1.6% by detailing compared to 0.4% by scaling in Figure 15).

The stator heat losses amount to 1.01% adiabatic rotor shaft power for the reference case and 1.17% for the future turbine. Using the formulation published by Atkins and Ainsworth [1], the loss of shaft power is predicted to be 0.19% for the reference case. Assuming unchanged adiabatic rotor power, the losses of the future turbine are 0.22%.

CONCLUSION

The presented heat loss model establishes a simple methodology for the estimation of end-wall heat losses in high-pressure turbines. The obtained heat losses per blade row can be used for efficiency analyses of the non-adiabatic engine cycle.

The first main goal of this work is to provide a model which is applicable during the whole design phase of a turbine, but especially in the early aerodynamic design phase. The scaled model requires little input data: only global quantities such as Reynolds number and average driving temperatures need to be known. The average thickness of solids is introduced by a rough estimate. However, heat losses of the validation case can be predicted with less than 5% error. It is therefore suited to be integrated in optimisation tools, e. g. for the one-dimensional annulus design.

In the course of the design process, the prediction quality of the scaled model might be insufficient. This leads to the second main goal of this work: The detailing procedure allows to continuously embed results of more complex aero-thermal computations. In situations like the mentioned example of casing treatments or the presented validation case, uncoupled CFD computations with iso-thermal wall boundary conditions can be used to get detailed knowledge of the heat transfer coefficients in regions of severe geometrical changes. The elaborated methodology allows to fill in these CFD results. Thereby, heat losses can be quickly estimated to judge the non-adiabatic efficiency gain of such design variations.

A further application of the elaborated method is that the heat resistance network can be used for improved boundary conditions in the aerodynamic design. Often, discrepancies in the near-wall region of CFD and experimental work are explained by the inadequate use of adiabatic walls. For partial CFD computations, e. g. pure main-flow or particular cavities, the ambient heat resistances of the model can be transformed into a mixed boundary condition. Firstly, the use of realistic mixed wall boundary conditions should improve the prediction of the near-wall flow. But secondly, it again enables the engineer to better compare design alternatives. In contrast to heat transfer coefficients obtained by CFD computations using arbitrary (mostly constant) Dirichlet or Neumann boundary conditions, the resulting heat flux can now be included in an energetic comparison.

The assumption of one-dimensional heat transfer through the solid elements is a significant drawback. The development of a scaling approach for rectangular two-dimensional solid elements in currently in progress. This is especially important for rotor disks. Furthermore, the scaling approach for the estimation of Nusselt numbers has to be extended by the effect of rotation.

Nevertheless, detailed aero-thermal models are still necessary and should be used as early as the design progress allows to set them up. The improvement of these models will remain an important research issue in the future.

ACKNOWLEDGMENT

The investigations presented in this paper were conducted as part of the LuFo IV program. The work was supported by the Bundesministerium für Wirtschaft und Technologie (BMWi) under grant number 20T0608A. The authors want to acknowledge Rolls-Royce Deutschland for their support and permission of publication. The responsibility for the content lies solely with its authors.

REFERENCES

[1] Atkins, N. R., and Ainsworth, R. W., 2007. “Turbine aerodynamic performance measurement under non-adiabatic conditions”. *ASME Conference Proceedings GT2007-27143*.

[2] Young, J. B., and Wilcock, R. C., 2002. “Modeling the air-cooled gas turbine: Part 1 — general thermodynamics”. *Journal of Turbomachinery*, ***124***(2), pp. 207–213.

[3] Young, J. B., and Wilcock, R. C., 2002. "Modeling the air-cooled gas turbine: Part 2 — coolant flows and losses". *Journal of Turbomachinery,* ***124***(2), pp. 214–221.

[4] El-Masri, M. A., 1986. "On thermodynamics of gas-turbine cycles: Part 2 — a model for expansion in cooled turbines". *Journal of Engineering for Gas Turbines and Power,* ***108***(1), pp. 151–159.

[5] Gülen, S. C., 2011. "A simple parametric model for the analysis of cooled gas turbines". *Journal of Engineering for Gas Turbines and Power,* ***133***(1), p. 011801.

[6] Sipatov, A., Gomzikov, L., Latyshev, V., and Gladysheva, N., 2009. "Thee dimensional heat transfer analysis of high pressure turbine blade". *ASME Conference Proceedings GR2009-59163*.

[7] He, L., and Oldfield, M. L. G., 2009. "Unsteady conjugate heat transfer modelling". *ASME Conference Proceedings GT2009-59174*.

[8] Okita, Y., and Yamawaki, S., 2002. "Conjugate heat transfer analysis of turbine rotor-stator system". *ASME Conference Proceedings GT2002-30615*.

[9] Okita, Y., 2006. "Transient thermal and flow field in a turbine disk rotor-stator system". *ASME Conference Proceedings GT2006-90033*.

[10] Lakshminarayana, B., 1996. *Fluid Dynamics and Heat Transfer of Turbomachineryang*. John Wiley & Sons, New York.

[11] Wilcock, R. C., Young, J. B., and Horlock, J. H., 2005. "The effect of turbine blade cooling on the cycle efficiency of gas turbine power cycles". *Journal of Engineering for Gas Turbines and Power,* ***127***(1), pp. 109–120.

[12] Kawaike, K., Kobayashi, N., and Ikeguchi, T., 1984. "Effect of new blade cooling system with minimized gas temperature dilution on gas turbine performance". *Journal of Engineering for Gas Turbines and Power,* ***106***(4), pp. 756–764.

[13] Kang, M. B., Kohli, A., and Thole, K. A., 1999. "Heat transfer and flowfield measurements in the leading edge region of a stator vane endwall". *Journal of Turbomachinery,* ***121***(3), pp. 558–568.

[14] Granovskiy, A., Kostege, M., Krupa, V., and Rudenko, S., 2007. "Influence of various casing design over a blade on a stage efficiency". *ISABE paper 2007-1343*.

[15] Arts, T., and Lambert de Rouvroit, M., 1992. "Aero-thermal performance of a two-dimensional highly loaded transonic turbine nozzle guide vane : a test case for inviscid and viscous flow computations". *Journal of Turbomachinery,* ***114***(1), pp. 147–154.

[16] Abu-Ghannam, B. J., and Shaw, R., 1980. "Natural transition of boundary layers – the effects of turbulence, pressure gradient, and flow history". *Journal of Mechanical Engineering Science,* ***22***(5), pp. 213–228.

[17] Menter, F. R., Langtry, R. B., Likki, S. R., Suzen, Y. B., Huang, P. G., and Völker, S., 2006. "A correlation-based transition model using local variables — part I: Model formulation". *Journal of Turbomachinery,* ***128***, pp. 413–422.

[18] Langtry, R. B., Menter, F. R., Likki, S. R., Suzen, Y. B., Huang, P. G., and Völker, S., 2006. "A correlation-based transition model using local variables — part II: Test cases and industrial applications". *Journal of Turbomachinery,* ***123***, pp. 423–434.

[19] Hylton, L. D., Mihelc, M. S., Turner, E. R., Nealy, D. A., and York, R. E., 1983. Analytical and experimental evaluation of the heat transfer distribution over the surfaces of turbine vanes. Tech. rep., NASA CR-168015.